ISSN 1063-7710, Acoustical Physics, 2010, Vol. 56, No. 2, pp. 158–167. © Pleiades Publishing, Ltd., 2010.
Published in Russian in Akusticheskiĭ Zhurnal, 2010, Vol. 56, No. 2, pp. 179–189.

NONLINEAR ACOUSTICS

Statistical Properties of Nonlinear Diffracting *N*-Wave behind a Random Phase Screen[1]

P. V. Yuldashev[a], N. A. Bryseva[a], M. V. Averiyanov[a], Ph. Blanc-Benon[b], and V. A. Khokhlova[a]

[a] *Department of Acoustics, Faculty of Physics, Moscow State University, Moscow, 119991 Russia*
[b] *LMFA, UMR CNRS 5509, Ecole Centrale de Lyon, 69134 Ecully Cedex, France*
e-mail: {petr,misha,vera}@acs366.phys.msu.ru, Philippe.Blanc-Benon@ec-lyon.fr

Received April 14, 2009

Abstract—Propagation of high amplitude *N*-wave behind a random phase screen is modeled based on the Khokhlov-Zabolotskaya-Kuznetsov equation. One-dimensional random phase screens with Gaussian power spectrum density are considered. The effects of nonlinear propagation, random focusing, and diffraction on the statistical properties of the acoustic field behind the screen, including propagation through caustics and beyond caustics, are analyzed. Statistical distributions and mean values of the acoustic field parameters obtained within the developed diffraction model and using nonlinear geometrical acoustics approach are compared.

DOI: 10.1134/S1063771010020065

1. INTRODUCTION

A model of an infinitely thin random phase screen has been widely used as a simplified approach to study various problems of linear and nonlinear wave propagation in random inhomogeneous media [1–5]. Contrary to the continuous inhomogeneous medium the phase screen model incorporates only initial distortion of the phase front of the wave. However, this model includes basic effects of nonlinear propagation and random focusing that lead to distortion of statistical characteristics of the wave field in randomly inhomogeneous medium. Propagation of high intensity noise through turbulent layers in the atmosphere is an example of where the phase screen model may be implemented. An ideal symmetrical *N*-wave is often used as an initial waveform of noise wave generated by the supersonic aircraft.

Up to date, the statistical properties of nonlinear *N*-waves behind a random phase screen were studied in detail using nonlinear geometrical acoustics (NGA) approximation [1–3]. The geometry of the problem in case of a one-dimensional screen is illustrated in Fig. 1. Initially plane *N*-wave propagates along the coordinate x perpendicular to the screen located at $x = 0$ [1]. At each transverse coordinate y the phase screen introduces a random time delay that leads to the distortion of the wave front. In NGA approach the spatial fluctuations of the time delay define areas of converging and diverging rays, i.e. focusing and defocusing of the wave (Fig. 1). Ray convergence corresponds to focusing, i.e. to the increase of the wave amplitude, and ray divergence corresponds to defocusing, i.e. decrease of the wave amplitude.

In NGA approximation the statistical properties of acoustic field behind the screen depend on the probability distribution function of ray convergence after passing the screen and the initial wave amplitude that determines nonlinear propagation effects. Analytic solutions have been obtained for probability distributions and mean values of the amplitude and duration of an *N*-wave after passing through one-dimensional phase screen having either broadband or narrowband Gaussian probability distribution of ray convergence [1]. The problem was farther extended and analytic

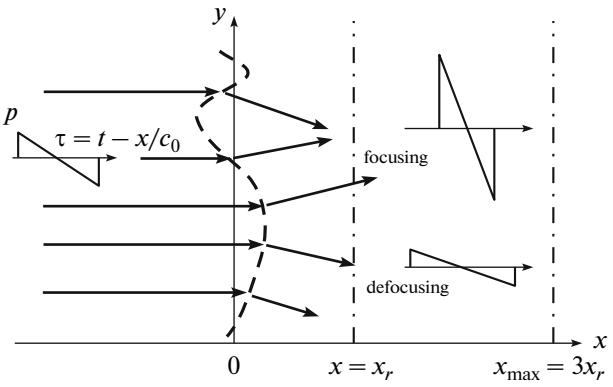

Fig. 1. Propagation of initially plane *N*-wave through infinitely thin phase screen (dashed line) located at $x = 0$. Arrows illustrate focusing and defocusing effects behind the screen. The refraction length is denoted as x_r, maximum propagation distance in numerical simulations is $x_{max} = 3x_r$.

[1] The article was translated by the authors.

solutions were obtained for non-perpendicular angle of incidence of a wave on the phase screen and for two-dimensional phase screens [2, 3]. The advantage of the NGA approach to this problem is that analytic solutions are available and basic physical effects can be clearly seen. However, some restrictions of the solutions call for developing of more general approaches. Here we list some of them. The NGA solutions are valid only at the distances before first caustics occur, i.e. some of the ray tube areas vanish to zero. Nonlinear amplitude dependence of the propagation speed of the *N*-wave shock front leads to additional distortions of the wave front in space. This effect may be considered within the NGA formulation, but the exact solution has not yet been obtained. The effects of diffraction are not included and therefore the wave keeps the *N*-waveform, although more variability of distorted waveforms like *U*-wave or double peaked and rounded waves may be expected [6]. Spatial pattern of the acoustic field behind the screen depends not only on the ray convergence probability function, but also on the characteristic size of the phase variations introduced by the screen. For small size random variations of the phase, focusing will occur from smaller spatial areas of the screen surface and for bigger size variations, from bigger apertures. If diffraction effects are of concern, for the same ray convergence, i.e. focal length to the caustics, the focusing gain in these two cases will be higher for bigger scale fluctuations. More statistical properties of the screen, in addition to the ray convergence distribution, therefore are necessary to adequately account for the diffraction effects while propagating through caustics.

In this paper, a model based on the numerical solution of the Khokhlov–Zabolotskaya–Kuznezov (KZK) equation is considered. This model accounts for the combined nonlinear and diffraction effects and makes it possible to consider wave propagation through and beyond caustics. Extended form of this equation is widely used in applications to the atmosphere acoustics to study propagation of finite amplitude acoustic waves in inhomogeneous media with continuous variations in space [7, 8]. Here, numerical simulations of *N*-wave propagation behind random realizations of one-dimensional screen are performed up to large distances further than the distance of occurrence of first caustics. Statistical properties of the phase screen are characterized by the phase probability distribution and by the spatial correlation function. The results of modeling are statistically analyzed and compared, where it is possible, with those calculated in nonlinear geometrical acoustics approximation [1, 3].

2. THEORY

2.1. Nonlinear Parabolic Model

The phase screen model is used here only to set initial time delays of the *N*-wave. The KZK equation for the wave propagation behind the screen in the homogeneous medium can be written in dimensionless form as follows:

$$\frac{\partial}{\partial\theta}\left[\frac{\partial P}{\partial\sigma} - NP\frac{\partial P}{\partial\theta} - A\frac{\partial^2 P}{\partial\theta^2}\right] = \frac{1}{4\pi}\frac{\partial^2 P}{\partial\rho^2}. \qquad (1)$$

Here $P = p/p_0$ is the acoustic pressure, normalized by the *N*-wave initial amplitude p_0, $\sigma = x/\lambda$ is the propagation distance, and $\rho = y/\lambda$ is the transverse spatial coordinate normalized by the *N*-wave length $\lambda = c_0 T_0$, c_0 is the ambient sound speed, $\theta = 2\pi\tau/T_0$ is the dimensionless time, normalized by the initial duration of the *N*-wave T_0, $\tau = t - x/c_0$ is the retarded time. Fluctuations of the time delay are introduced at $\sigma = 0$ in one spatial direction ρ, therefore the Laplacian diffraction term in the right hand side of the Eq. (1) is applied over this coordinate only. Dimensionless parameters are introduced as $N = 2\pi\varepsilon p_0/c_0^2\rho_0 = \pi\lambda/x_n$ is nonlinear parameter, where $x_n = T_0 c_0^3\rho_0/2\varepsilon\rho_0$ is the characteristic nonlinear distance at which the amplitude of the plane *N*-wave decreases by a factor of $\sqrt{2}$, ε is the nonlinearity coefficient of the propagation medium, $A = (2\pi)^2 c_0^2\delta/\lambda \ll 1$ is the thermoviscous dissipation parameter, δ is the coefficient of the diffusivity of sound.

Single *N*-wave with a random time delay $2\pi\Psi(\rho)$ at each transverse coordinate is considered as a boundary condition, i.e., $P(\sigma = 0,\theta,\rho) = P_0(\theta - 2\pi\Psi(\rho))$, where $P_0(\theta)$ is the *N*-wave of an amplitude of one and duration is 2π. Phase shift $\Psi(\rho)$ is chosen according to particular random realization of the phase screen used in simulation. Since weak dissipation is taken into account in the modeling, shock front of the *N*-wave is not infinitely thin and rise time is defined here as the time required for the pressure to increase from 10 to 90% of the maximum peak pressure. The initial rise time is chosen according to the quasi-stationary solution to the Burgers equation with given parameters *A* and *N*, and is approximately equal to $10A/N$. The initial *N*-wave at $\sigma = 0$ thus is constructed as a combination of an ideal *N*-wave (zero rise time, unit amplitude) with the fronts smoothed according to the values of absorption and nonlinearity parameters, *A* and *N*. As a result of such smoothing, peak pressures in the initial *N*-wave is slightly smaller than that of the ideal one. However, this difference does not exceed 8% for the simulation parameters used in this paper.

Numerical solution to the Eq. (1) is obtained using an algorithm developed in our previously studies [7]. Briefly this numerical time domain algorithm is based on the method of fractional steps with a first-order operator-splitting procedure, so that nonlinear, absorption, and diffraction effects are applied sequentially over a grid step in the propagation coordinate. Diffraction and absorption operator are solved using Crank–Nicolson finite difference method. Nonlinear

operator was integrated using conservative Godunov-type algorithm [9]. A boundary condition at the edges of the transverse spatial grid $\rho = 0$ and $\rho = L$, where L is the length of the screen, is chosen as $\partial P/\partial\rho = 0$. To control reflections from the boundaries the fluctuations introduced by the phase screen at $\sigma = 0$ are set to zero in the vicinity of the boundaries, so that the N-wave has a plane wave front in the regions $[0, L_0]$ and $[L - L_0, L]$, where $L_0 \ll L$. The computational domain in the transverse coordinate is chosen large enough in order, first, to avoid undesirable reflections from the boundaries at the propagation distances considered and, second, to have sufficiently large working region for computation of statistical distributions with minimal statistical error. Typically, numerical simulations are performed for a random phase screen with the width equal to 700λ and up to the distances of several nonlinear lengths, the time window changes from $\theta = -9.5$ to $\theta = 28$, which yields approximately 6 periods of the initial N-wave. Numerical steps are chosen according to the considered dimensionless parameters in the Eq. (1). In the case of absorption parameter equal to $A = 1.5 \times 10^{-4}$ and nonlinearity parameter equal to $N = 0.05$, the numerical step along the transverse coordinate is equal to $h_\rho = 0.01$, time step is equal to $h_\theta = 0.009$ and numerical step in the propagation direction is equal to $h_\sigma = 0.025$. The dissipation parameter A is chosen in the way to maintain the stability of the numerical algorithm for the range of nonlinear parameters N considered here and remains unchanged.

2.2. Phase Screen Model

Statistical properties of continuous randomly inhomogeneous media depend on a spatial power spectrum of fluctuations. The spatial power spectrum of the phase screen is usually derived from the spectrum of continuous random medium thus retaining its characteristic properties. To model the atmospheric turbulence the von Kármán, Kolmogorov, and Gaussian power spectra are commonly used [10]. Kolmogorov energy spectrum describes turbulent energy distribution inside the inertial interval enclosed between outer and inner scales, but does not give information about spectrum distribution outside this region. A more realistic model is the von Kármán model. It is also a two scale model that, in addition to the inertial interval, describes turbulent energy behavior at small wave numbers and its dissipation at large wave numbers. For atmospheric turbulence, the ratio between the internal and external scales is very small (less than 0.001) and this impose some restrictions to the wave propagation modeling [10, 11]. The small turbulent structures in the Kolmogorov or von Kármán spectra which are smaller than the acoustic wavelength produce backward scattering which is not taken into account in the KZK equation. In the modeling, therefore, a spectrum should be used, in which small scale fluctuations, less than the wave amplitude, are suppressed.

Spatial energy spectrum of the Gaussian shape describes fluctuations of one characteristic scale. If this scale is chosen equal to the outer scale of a real turbulence, we suppress small scale inhomogeneities, thus retaining the validity of the parabolic approximation. Although Gaussian spectrum does not exactly correspond to a realistic atmospheric turbulence, it is a very convenient and is widely used model [4, 5, 12]. Here we stay within the frame of the Gaussian formalism, which is sufficient for the aim to investigate the effect of the inhomogeneity scale on the N-wave propagation regardless multiple scales phenomena.

Random realizations of the phase screen were obtained using well-known method of filtering white Gaussian noise to fit the second-order statistics of the random phase $\Psi(\rho)$ [4, 5, 11]. In this method the amplitude of each harmonic of the discrete Fourier spectrum of the function $\Psi(\rho)$ is taken as δ-correlated pseudorandom normally distributed complex number, multiplied by the factor $\sqrt{G(k = n\Delta k)\Delta k}$, where

$$G(k) = G_0 \exp(-k^2 l^2/2) \tag{2}$$

is the Gaussian power spectrum density of the screen $\Psi(\rho)$, G_0 is the amplitude of the spectrum, l is the correlation length of the screen or the characteristic spatial scale of phase inhomogeneities, n is the number of discrete spatial harmonic, Δk is the discretization step between the harmonics. Then the inverse discrete Fourier transform is performed and yields two statistically independent realizations of the phase screen, $\Psi(\rho)$, which are the real and imaginary parts of the transformation result. The phase fluctuations $\Psi(\rho)$ have Gaussian statistics with zero average value and standard deviation D_0:

$$W(\Psi) = 1/\sqrt{2\pi D_0^2}\exp\left(-\Psi^2/2D_0^2\right). \tag{3}$$

The second spatial derivative of the phase, $\partial^2\Psi/\partial\rho^2$, determines the convergence of the ray tube at each transverse coordinate ρ and also has Gaussian distribution law [1]:

$$W\left(\Psi'' = \partial^2\Psi/\partial\rho^2\right) = 1/\sqrt{2\pi D_2^2}\exp\left(-\Psi''^2/2D_2^2\right). \tag{4}$$

The inverse value of the standard deviation D_2 of the distribution, Eq. (4), is the characteristic refraction length $\sigma_r = 1/D_2$, which is the distance from the phase screen where most of the first caustics occur. Since the KZK equation well describes only paraxial wave propagation and small angles of diffraction [13], the refraction length in simulations is chosen sufficiently large in comparison to the N-wave wavelength and the correlation length: $\sigma_r = x_r/\lambda = 63$.

In the solutions, obtained using NGA approach, all statistical properties of nonlinear acoustical field at a

chosen distance from the screen depend only on the ratio between characteristic refraction σ_r and nonlinear $\sigma_n = x_n/\lambda$ lengths [1, 2]. If diffraction effects are taken into account, additional parameters, the ratio of the *N*-wave length and the correlation length of the phase screen, are of importance.

Gaussian power spectrum density, Eq. (2), is characterized by two independent parameters: the amplitude G_0 and the correlation length l. According to the basic properties of Gaussian processes, the characteristic refraction length σ_r is related to the chosen parameters G_0 and l as:

$$\sigma_r^{-2} = 3\sqrt{2\pi}l^{-5}G_0. \quad (5)$$

Two typical phase screen realizations with the same characteristic refraction length σ_r but different correlation lengths are presented on the left side in Fig. 2. Correlation lengths are normalized by the length of an initial *N*-wave. The realization, Fig. 2a, has the correlation length $l = 3$, and the realization, Fig. 2b, has twice bigger spatial scale, $l = 6$. The choice of the spatial scales of fluctuations corresponds to the experimental data [6]. It is seen that the phase fluctuations of the second screen (Fig. 2b) with larger spatial variations are bigger in amplitude than those of the screen with smaller scale variations (Fig. 2a). It can be easily explained using the basic properties of the Gaussian processes. The amplitude of phase fluctuations is proportional to the dispersion D_0, Eq. (3), which satisfies the relation $D_0^2 = \sqrt{2\pi}G_0/l$ in the case of the Gaussian spectrum Eq. (2). Substituting this relation into the Eq. (5) and eliminating the spectrum intensity G_0, we obtain that $D_0 = l^2/\sigma_r\sqrt{3}$, i.e., the dispersion of phase fluctuations is proportional to the square of the correlation length. Phase fluctuations from the second screen are therefore more intensive than those from the first one, which is observed in Fig. 2. In the NGA approach these two phase screens of the same refraction length are equivalent in statistical sense and produce equivalent statistical solutions for the *N*-wave amplitude. However, if diffraction effects are considered, the solutions will be different. For example, phase fluctuations that are spatially bigger should produce stronger focusing in caustics.

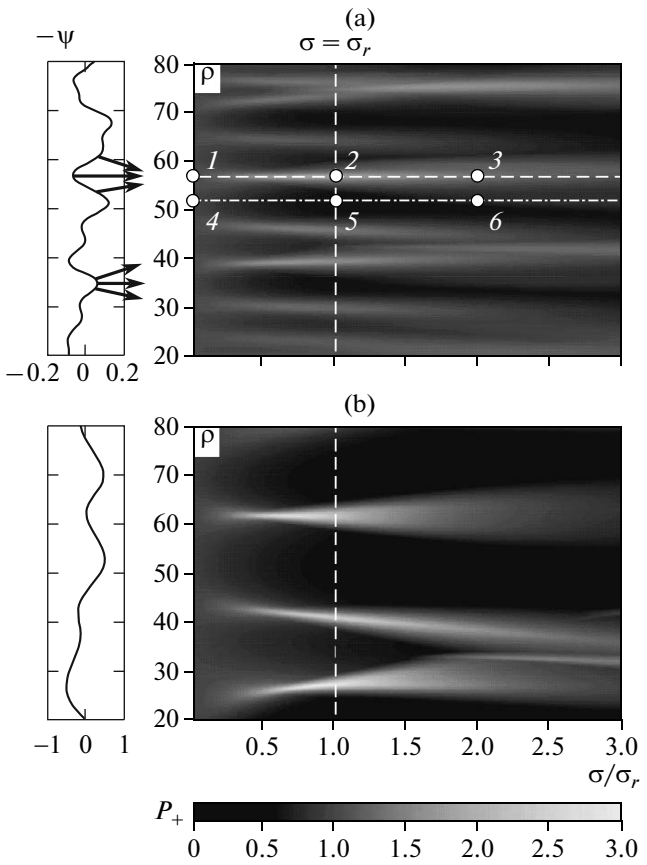

Fig. 2. Spatial distributions of the peak positive pressure for initially plane *N*-wave propagating behind two different random phase screens $\Psi(\rho)$ shown as solid curves on the left. Correlation length l of the screens is (a) $l = 3$ and (b) $l = 6$. Nonlinear length $\sigma_n = 8\sigma_r$, refraction length $\sigma_r = 63$. *N*-waveforms calculated along the horizontal dash line (through focusing zone) at points *1–3* are shown in Fig. 4a and calculated along the horizontal dash-dot line (through defocusing zone) at points *4–6* are shown in Fig. 4b. Peak pressure along vertical dashed line on Fig. 2a is presented in Fig. 3b.

3. RESULTS

In this paper, the probability distribution functions of acoustic field were calculated from a few realizations of the phase screen sufficiently wide in the y direction. According to the hypothesis of ergodicity, this is equivalent to the average over a large number of realizations in one spatial point. For each value of nonlinear parameter N, acoustic field modeling was performed using two statistically independent realizations of the phase screen. The length of each realization was equal to 700λ or approximately 100 and 50 characteristic scales of phase fluctuations for the screens with $l = 3$ and $l = 6$, respectively. Comparison between statistical distributions of the acoustic field modeled with these two independent phase screens showed a good agreement and justify that the chosen length of phase screens was long enough for statistical analysis.

Typical spatial patterns of the *N*-wave peak positive pressure, P_+, measured behind two phase screens of the same refraction length but smaller or bigger correlation lengths, are illustrated in Figs. 2a and 2b. Phase screens are presented on the same figure as an initial phase shift of the acoustic wave. For a better visualization of the process we plotted a zoom, the width of the regions shown in the figure is much smaller than the real computational domain. Dimensionless nonlinear length equal to $\sigma_n = 8\sigma_r$ and dimensionless refraction

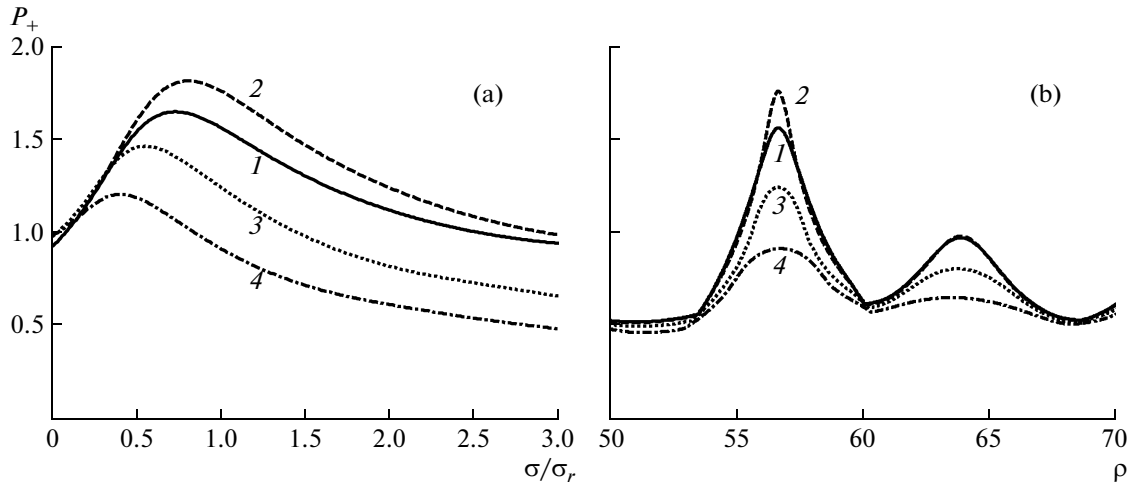

Fig. 3. Evolution of the peak positive pressure along the horizontal (through focusing zone) (a) and vertical (b) dashed lines in Fig. 2a for different nonlinear lengths: (*1*) $\sigma_n = \infty$ (linear), (*2*) $\sigma_n = 8\sigma_r$, (*3*) $\sigma_n = 2\sigma_r$ and (*4*) $\sigma_n = \sigma_r$. Curve *2* corresponds to the pattern shown in Fig. 2a.

length equal to $\sigma_r = 63$ were used to calculate both patterns. Dimensionless correlation lengths of the screens were $l = 3$ (Fig. 2a) and $l = 6$ (Fig. 2b). Arrows in Fig. 2a illustrate focusing or defocusing of acoustic wave according to the advance or delay of the initial phase (convex and concave regions of the phase screen). Complex spatial structure of the acoustic field is observed: focal zones form at different distances from the phase screen and have different focusing gains, depending on the size and strength of the particular phase inhomogeneity of the screen. The first high amplitude focusing regions (in general, caustics) are located at the distance approximately equal to the refraction length σ_r. This distance is shown with the vertical dashed line. At distances greater than the refraction length, formation of random foci is observed as well as the result of focusing produced by less probable large scale phase fluctuations. On average the amplitude of the *N*-wave in these foci is smaller than in the first ones mainly due to nonlinear dissipation effect, but also due to the thermoviscous absorption. Comparison of Figs. 2a and 2b shows that focusing effects are more pronounced for the phase screen with fluctuations of larger spatial correlation scale. For example, the maximum dimensionless pressure in the first acoustic pattern is equal to $P_+ = 1.8$ and in the second one, to $P_+ = 3.1$. However, less number of foci is observed behind the screen with a large correlation length. Smaller scale phase modulation of the wave front thus result in bigger number of random foci of less peak pressure as compared to larger scale phase modulation of the same refraction length.

Focusing gain in caustics is affected also by nonlinear effects. Linear *N*-wave propagation is considered here as a reference case. If nonlinear effects are sufficiently strong, they lead to strong nonlinear dissipation at the wave shock front and the *N*-wave amplitude decays rapidly during its propagation from the phase screen to the caustic. On the other hand, nonlinear steepening of the shock front at high amplitude field regions enhances focusing, since the acoustic wave differentiates in the caustic (with some correction on the absorption and nonlinear effects). This nonlinear enhancement of focusing will dominate over the nonlinear dissipation for the moderate initial *N*-wave amplitudes. Inversely, if initial amplitude is very high, the effect of focusing will be weaker for nonlinear propagation than for the linear one. The efficacy of focusing in the caustic depends therefore on the value of the refraction length and is a nonmonotonic function of the characteristic initial wave amplitude.

This nonmonotonic behavior of the focusing gain is illustrated in Figs. 3a and 3b. The distributions of the peak positive pressure are shown along the propagation coordinate σ in Fig. 3a. The transverse coordinate is fixed at $\rho = 56.7$ as marked in Fig. 2a with the horizontal dashed line. This chosen trajectory passes through the caustic. Shown in Fig. 3b are the peak pressure distributions along the transverse coordinate ρ at the distance of refraction length $\sigma = \sigma_r$ as marked in Fig. 2a with the vertical dashed line. Linear propagation and three nonlinear regimes are considered. Solid curve *1* corresponds to the linear regime and the nonlinear regimes have the following characteristic nonlinear lengths: $\sigma_n = 8\sigma_r$, dashed line *2*; $\sigma_n = 2\sigma_r$, dotted line *3*; and $\sigma_n = \sigma_r$, dash–dotted line *4*. In each nonlinear case the initial waveform is defined according to the quasi-stationary solution as discussed above. In the case of linear propagation the initial waveform is identical to the waveform in the case of lowest amplitude nonlinear propagation, $\sigma_n = 8\sigma_r$. It is seen that for $\sigma_n = 8\sigma_r$, case *2*, the peak pressure in the focus exceeds the linear one approximately by 10%. In the

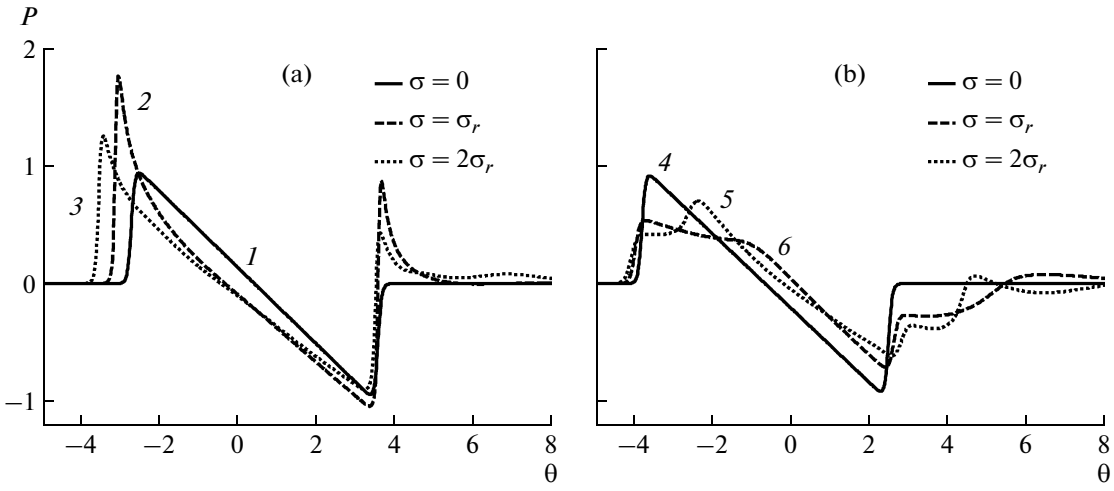

Fig. 4. Initial and distorted *N*-waveforms modeled at points *1–3* and *4–6* along the horizontal dashed (a) and dash-dot (b) lines shown in Fig. 2a. Waveforms are consequently numbered: initial waveform (solid curves *1* and *4*), in the focus (dashed curve *2*, $\sigma = \sigma_r$), and after the focus (dotted curve *3*, $\sigma = 2\sigma_r$). In defocusing zone double peaked waveform (dotted curve *5*) and rounded waveform (dashed curve *6*) are observed.

cases *3* and *4* nonlinear effects are too strong, nonlinear absorption at the shocks dominates over nonlinear enhancement of focusing, peak pressure is lower than in the linear case and decreases when nonlinear effects increase. A conventional shift of the peak pressure maximum toward the phase screen for smaller nonlinear lengths (increase of the initial wave amplitude) is observed.

Distortion of the initial *N*-shape of the wave due to the combined effect of diffraction, nonlinearity, and random focusing is illustrated in Fig. 4. The waveforms were calculated at different propagation distances from the screen along two horizontal lines shown in white in Fig. 2a. The dashed line passes through a random caustic and dash-dotted line passes through the lower amplitude defocusing zone. Particular points on the lines at which waveforms are grasped are marked by white circles and numeration of circles corresponds to numeration of waveforms in Fig. 4. The initial *N*-wave is plotted as solid curves *1* and *4*. Typical waveform modifications observed while propagating through the caustic are shown in Fig. 4a: in the focal zone ($\sigma = \sigma_r$) the waveform tends to take asymmetric *U*-shape (dashed curve *2*) with higher peak positive pressure; at longer distance $\sigma = 2\sigma_r$, the waveform (dotted curve *3*) has lower amplitude, long pressure tail and longer duration due to nonlinear effects. Waveform distortion when propagating through the defocusing zone is shown in Fig. 4b: double peaked (dotted curve *5*) and rounded (dashed curve *6*) waveforms are observed due to the interference of waves having slightly different arrival times due to scattering from the preceding foci.

Statistical properties of the *N*-wave field behind the screen are described here by probability distribution function of the peak positive pressure, P_+. To compute statistical distributions, the results of acoustic field modeling behind two independent realizations of random phase screen were used. For each step in propagation distance σ from the screen, pressure amplitudes P_+ were calculated in every spatial transverse grid point and the probability $W(P_+)dP_+$ was calculated proportionally to the number of points with amplitudes fitting the interval from P_+ to $P_+ + dP_+$. Characteristic nonlinear and refraction lengths were chosen equal, $\sigma_n = \sigma_r$. The results of calculations are shown in Figs. 5a, 5b and 5c for the distances $\sigma = 0.25\sigma_r$ (a), $\sigma = \sigma_r$ (b), and $\sigma = 2\sigma_r$ (c) from the phase screen. For comparison, analytic solutions (solid curves) for the pressure amplitude distributions obtained using the NGA approximation are also shown [1]. Note that these solutions are only valid for distances shorter than the refraction length. Thin black curves and circle markers correspond to the KZK numerical solution for the random phase screen with correlation length equal to $l = 3$. Thin gray lines and gray circle markers correspond to the results for the screen of correlation length $l = 6$. *N*-wave amplitudes in case of nonlinear plane wave propagation, without any initial phase modulation, are shown as vertical dashed lines. The results of both KZK modeling and NGA calculations show broadening of the initial δ-function distribution of the *N*-wave amplitude. It is seen that at short distances from the phase screen ($\sigma = 0.25\sigma_r$, Fig. 5a) probability distributions obtained with NGA approach and KZK modeling for both screens are very similar: in prefocal zone the effect of diffraction and of the correlation length is almost negligible.

At longer distances ($\sigma = \sigma_r$, Fig. 5b), the results of NGA and KZK modeling become different. Most of the gray curve (large scale) is still close to the predic-

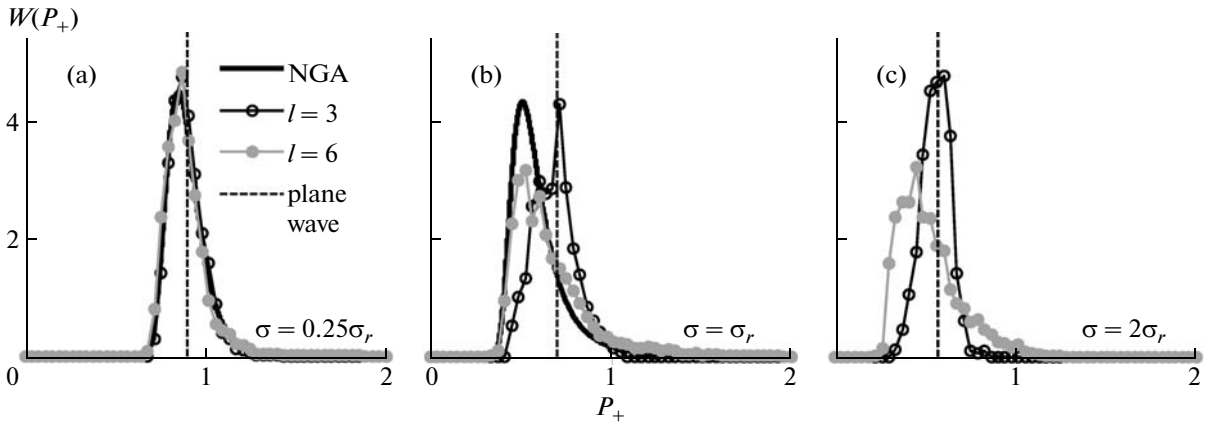

Fig. 5. Comparison between probability distribution functions of the *N*-wave peak positive pressure obtained using the KZK numerical model (circle markers) and analytical solution in the NGA approach [1] (solid lines). Black circle markers correspond to the phase screen with correlation length $l = 3$ and gray circle markers, $l = 6$. Dashed lines—distributions for nonlinear plane wave propagation (δ-functions). The distributions are presented for distances $\sigma = 0.25\sigma_r$, (curve (a)), σ_r, (curve (b)) and $2\sigma_r$, (curve (c)) behind the phase screen. Nonlinear length is $\sigma_n = \sigma_r$ and refraction length is $\sigma_r = 63$.

tions of the NGA approach. The distributions at low amplitudes that correspond to the divergent zones of the field (Fig. 2a), agree reasonably well. This means that the waveforms in these regions predicted with and without account for diffraction effects are surprisingly close in amplitude. Small number of high amplitude focal zones occupy spatially small portion of the transverse cross section of the field (Fig. 2a) and thus give small contribution to the probability density. This part of the distribution of high amplitudes is long but relatively small in both models. However, if some random focus forms close to, but before the distance of interest, the probability of high field values from this focus is lost in the NGA solution, but is included in the diffraction model. The results obtained from the diffraction model (gray curve) are therefore higher than in the NGA solution (solid curve). NGA approximation also yields an overestimation of the maximum value of the probability distribution as compared to the KZK model. This is again due to the fact that the NGA approximation neglects already converged ray tubes. As the phase screen has a random nature some of the caustics appear at short distances than the refraction length σ_r. Ray tubes converged to these caustics are excluded from calculations, total number of rays taken into account decreases, the probability density becomes relatively higher and looses its normalization with propagation distance.

In the case of small-scale inhomogeneities (black curve with circle markers in Fig. 5b) the diffraction effects act much stronger. No strong focusing occurs (Fig. 2a), so the probability to observe very high amplitudes is smaller than for the large scale focusing (Fig. 2b). On the other hand, the number of random foci is bigger, so the probability to observe increased pressures is relatively higher than in the case of small number of foci. The distribution is shifted to higher amplitudes and lies almost symmetrically around the regular value that corresponds to the nonlinear plane wave propagation. Small scale phase modulations therefore yields broadening of the *N*-function distribution of the regular *N*-wave, but results in less shift of the distribution towards smaller amplitudes as compared to the large scale modulation. This difference of the effect of inhomogeneities of either large of small size is even better seen at longer distances from the screen as shown in Fig. 5c. Here the distance is equal to two refraction lengths, $\sigma = 2\sigma_r$, and NGA solution is no longer valid; the results are presented only for the KZK equation modeling. Again, large-scale phase screen results in higher probability to observe high peak pressures, but the maximum of probability density is shifted towards low amplitude values as compared to the small-scale phase screen.

The effect of nonlinearity on statistical distributions of the peak pressure is illustrated in Fig. 6. Linear wave propagation (Fig. 6a), nonlinear propagation with $\sigma_n = 4\sigma_r$ (Fig. 6b) and stronger nonlinear effects with $\sigma_n = \sigma_r$ (Fig. 6c) are considered at the distance of two refraction lengths, $\sigma = 2\sigma_r$, from the screen. Correlation length is equal to $l = 3$. It is seen that stronger nonlinearity leads to narrowing the statistical distribution. For example, in the linear case, statistical distribution is about twice wider than in the strongest nonlinear case (Fig. 6c). In addition, the latter distribution has very short pressure tail at high amplitudes. Nonlinear effects thus suppress fluctuations of acoustic field induced by the initial distortion of wave front. This is the result of increased nonlinear absorption in focusing zones that leads to faster amplitude decay and thus to faster quieting of high amplitudes.

Quantitatively, the combined effects nonlinearity and random focusing can be analyzed by comparing first two statistical momentums: mean value and stan-

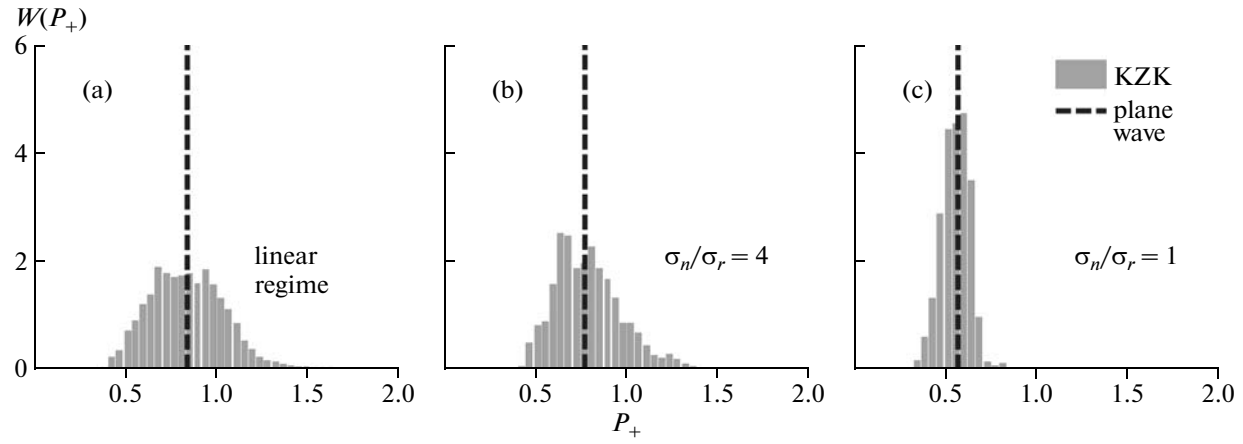

Fig. 6. Comparison between probability distribution functions of the *N*-wave peak positive pressure obtained at the distance $\sigma = 2\sigma_r$ for correlation length $l = 3$ and for various nonlinear lengths σ_n: linear (a); $\sigma_n = 4\sigma_r$ (b) and $\sigma_n = \sigma_r$ (c).

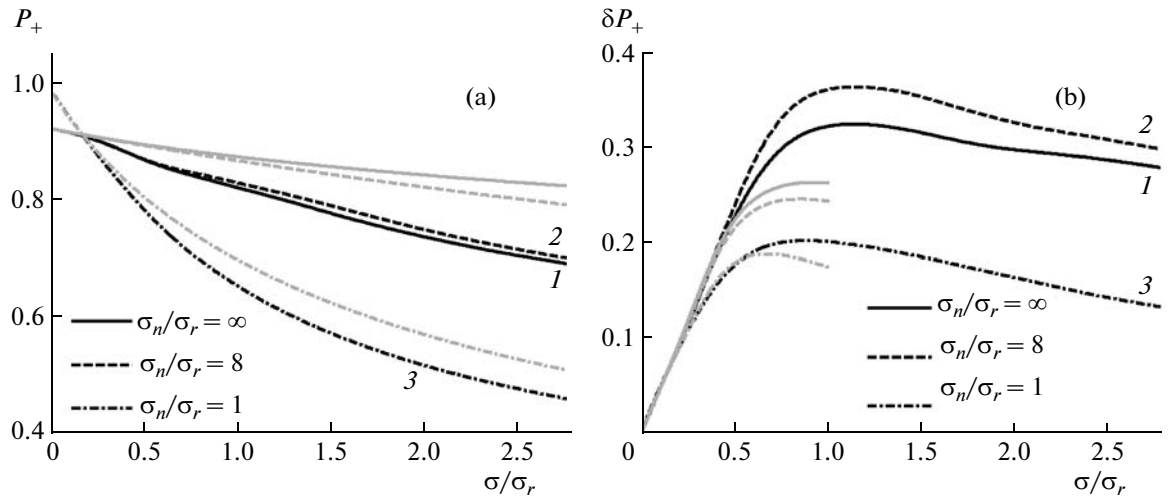

Fig. 7. Averaged peak positive pressure (a) and its standard deviation (b) as a function of propagation distance for various nonlinear lengths σ_n: solid—linear, dashed—nonlinear $\sigma_n = 8\sigma_r$ and dash-dotted—nonlinear $\sigma_n = \sigma_r$ (curve *3*). Gray curves in (a) correspond to the plane *N*-wave propagation. Gray curves in (b) correspond to the analytical solution in NGA approximation.

dard deviation of the peak pressure. In Figs. 7a and 7b the mean value and standard deviation of the amplitude along the propagation coordinate are presented. Refraction length is equal to $\sigma_r = 63$ and correlation length is equal to $l = 6$ (large scale inhomogeneities). Black curves in both (a) and (b) correspond to propagation of randomly modulated wave, solid curves *1* correspond to linear propagation, dashed curves *2* correspond to nonlinear propagation with $\sigma_n = 8\sigma_r$, and dash-dotted curves *3* correspond to nonlinear propagation with $\sigma_n = \sigma_r$. A set of three gray lines in Fig. 7a corresponds to the plane wave propagation without phase modulation. In Fig. 7b a set of three gray lines corresponds to the standard deviations obtained in the NGA approximation up to the distance of one refraction length, where the NGA solutions are valid.

It is seen that the presence of phase screen yields lower mean amplitudes than those in case of plane wave propagation (Fig. 7a), as it would be expected from the distributions shown in Fig. 5. Weak nonlinearity leads to slightly higher mean amplitudes of randomly modulated wave than in the case of its linear propagation. Similarly to the case of a single focus, shown in Fig. 3, focusing is more effective for steeper shocks, produced by nonlinear propagation and this effect dominates over nonlinear dissipation. For the regular plane wave, evidently, the effect is the opposite as nonlinearity induces additional dissipation only: mean amplitudes are higher for the linear field. In the case of strong nonlinear effects, the mean amplitudes are much lower than for the linear wave both in the random and plane wave fields because of the strong nonlinear absorption at the shock.

The behavior of the standard amplitude deviation with propagation distance is nonmonotonic, as shown in Fig. 7b. The results are presented for the random field only as standard deviation is zero for the plane wave propagation. At first, standard amplitude deviation grows linearly from its zero value at $\sigma = 0$. This linear growth is the same for all nonlinear lengths, that is consistent with the asymptotic solution, derived using NGA approximation: $\delta P_+ = 0.5\sigma/\sigma_r$, if $\sigma \ll \sigma_r$. The deviation has a maximum at the distance approximately equal to the refraction length. In fact, most intensive focusing is observed at this length and thus leads to broadening of the probability distribution. Further the standard deviation decreases slowly and monotonically with the distance of propagation. It is seen that for linear regime (curve *1*) and weak nonlinearity (curve *2*) the maxima of standard deviations are located very close to the distance of one refraction length from the screen. Stronger nonlinearity (curve *3*) results in a shift of the maximum towards the phase screen due to the mechanism of nonlinear absorption, which suppresses high amplitudes. Maximum value of standard deviation is also non-monotonic with increasing nonlinearity as it takes place for the mean amplitude. Weak nonlinearity (curve *2*) results in slightly greater maximum than in the linear case (curve *1*). Strong nonlinearity significantly decreases the maxima and the overall level of standard deviation (curve *3*) as it was also seen in Fig. 6. The fluctuations of peak positive pressure in a random field are suppressed for high amplitude waves to strong nonlinear absorption at the shocks especially in the focusing zones.

On Fig. 7b we also compare standard amplitude deviations obtained either from the KZK modeling or from the analytic solutions of the NGA approach (gray curves) for different values of nonlinear propagation distance. Note that according to the discussion of Fig. 5b the comparison here is provided for renormalized probability densities of the NGA solution: $\tilde{W}(P_+) = W(P_+)/\int_0^\infty W(P_+)dP_+$. It is seen, that after the distance of $\sigma = 0.5\sigma_r$ curves calculated in NGA approximation become different from the KZK solution. If renormalization to keep the integral of the probability density equal to unit is not applied, the difference become noticeable after the distance of $\sigma = 0.25\sigma_r$. For longer distances, closer to refraction length, the NGA solution is no longer valid and becomes quite different from the diffraction model.

4. CONCLUSIONS

The combined effects of nonlinearity, random focusing, and diffraction on *N*-wave propagation behind a random phase screen are investigated using the KZK equation. Probability distributions and mean values of the *N*-wave amplitude are obtained from the numerical solutions of the KZK equation and are presented for various initial wave amplitude and various distances from the phase screen, including propagation through caustics. The effect of the spatial size of phase fluctuations on statistical distributions is considered. Results obtained from the KZK diffraction model are compared with analytical predictions of the NGA approach.

It is shown that close to the screen, or quantitatively up to the distances of $\sigma = 0.5\sigma_r$, the results of the diffraction and geometric approaches agree very well. At longer distances statistical properties of the random acoustic field can be accurately described only if diffraction effects are taken into account. First major focusing zones (caustics) form on average at one refraction distance σ_r. This distance fully characterizes the focusing properties of the screen in the NGA approach. However, the KZK diffraction model shown that phase screens of the same refraction length, statistically the same for the NGA approach, produce random acoustic fields with quite different statistical properties, if phase fluctuations have different spatial scales. Contrary to the NGA model that saves *N*-waveform everywhere, the diffraction model predicts more realistic waveforms that are characteristic for *N*-wave propagation in inhomogeneous media. For example, *U*-shape waves occur in caustics, rounded and double peaked waves, in defocusing zones.

The effect of diffraction, while propagating through and after random foci, yields smoothening the spatial structure of a random acoustic field and therefore narrowing the probability distributions of peak pressure around its average value. These effects are stronger for smaller scale fluctuations. The effect of nonlinearity is non-monotonic. Weak nonlinearity leads to slight enhancement of focusing effects resulting in higher amplitude regions and, as consequence, in additional broadening of the probability distributions towards high values of amplitudes, bigger mean values and standard deviations as compared to the linear case. Strong nonlinear effects suppress amplitude fluctuations and lead to narrower probability distributions, smaller mean values and standard deviations.

ACKNOWLEDGMENTS

This work was partially supported by RTBR and INTAS 05-1000008-7841 grants.

REFERENCES

1. A. N. Dubrovskii, V. A. Khokhlova, and O. V. Rudenko, Akust. Zh. **42**, 550 (1996) [Acoust. Phys. **42**, 550 (1996)].
2. V. A. Gusev and O. V. Rudenko, Akust. Zh. **52**, 24 (2006) [Acoust. Phys. **52**, 24 (2006)].

3. O. V. Rudenko and B. O. Enflo, Acta Acust., Acustica **86**, 229 (2000).
4. S. A. Shlenov and V. P. Kandidov, Opt. Atmos. Okeana **17**, 565 (2004).
5. J. M. Martin and S. M. Flatté, Appl. Opt. **27**, 2111 (1988).
6. B. Lipkens, J. Acoust. Soc. Am. **103**, 148 (1998).
7. M. V. Averiyanov, V. A. Khokhlova, O. A. Sapozhnikov, Ph. Blanc-Benon, and R. O. Cleveland, Akust. Zh. **52**, 623 (2006) [Acoust. Phys. **52**, 623 (2006)].
8. M. V. Averiyanov, V. A. Khokhlova, R. O. Cleveland, and Ph. Blanc-Benon, in *Proc. of the 19th RAO Session* (GEOS, Moscow, 2007), Vol. 1, pp. 147–151.
9. A. Kurganov and E. Tadmor, J. Comp. Phys. **160**, 241 (2000).
10. S. M. Rytov, Yu. A. Kravtsov, and V. I. Tatarskii, *Introduction to Statistical Radio Physics* (Nauka, Moscow, 1978), Part 2 [in Russian].
11. A. M. Vorontsov, P. V. Paramonov, M. T. Valley, and M. A. Vorontsov, Waves Random Complex Media **18**, 91 (2008).
12. Ph. Blanc-Benon, B. Lipkens, L. Dallois, M. F. Hamilton, and D. T. Blackstock, J. Acoust. Soc. Am. **111**, 487 (2002).
13. J. N. Tjotta, S. Tjotta, and E. H. Vefring, J. Acoust. Soc. Am. **89**, 1017 (1991).